# Supplementary information
## Preparation of graphene bilayers on platinum by sequential chemical vapour deposition

*Johannes Halle*, Alexander Mehler, Nicolas Néel, Jörg Kröger*
Institut für Physik, Technische Universität Ilmenau, D-98693 Ilmenau, Germany
E-mail: johannes.halle@tu-ilmenau.de

November 29, 2018

## 1 Intercalation of deposited Pt film

In order to further evidence that the buried monolayer graphene (MLG) forms the bottom layer in bilayer graphene (BLG), Fig. S1 demonstrates the entire intercalation of the thick Pt film through the buried MLG. Upon annealing the Pt-covered MLG/Pt(111) sample (Fig. S1a) at 1200 K, the deposited Pt is flattening and intercalating under MLG (Fig. S1b,c). The segregated MLG exhbits the characteristic moiré pattern (Fig. S1d).

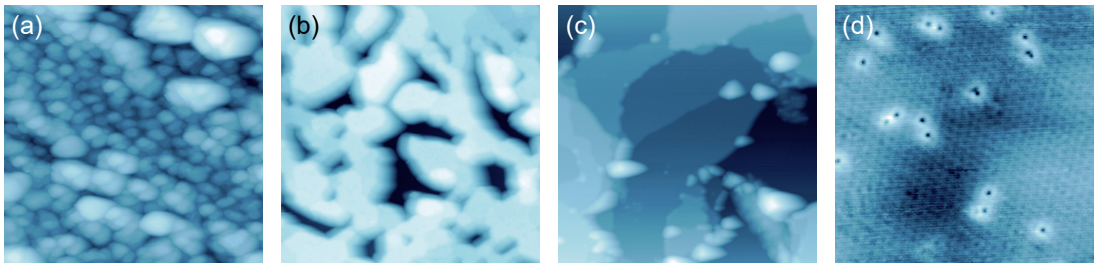


Figure S1: Pt intercalation of MLG-covered Pt(111). (a) STM image of Pt film deposited on MLG/Pt(111) (1 V, 80 pA, $120 \times 120\,\mathrm{nm}^2$). (b) STM image of the deposited Pt smoothed by annealing at 720 K (1.5 V, 80 pA, $150 \times 150\,\mathrm{nm}^2$). (c) STM image of MLG/Pt(111) after complete intercalation of the deposited Pt at 1200 K (1.5 V, 80 pA, $100 \times 100\,\mathrm{nm}^2$). (d) MLG moiré pattern observed on the sample shown in (c) (0.1 V, 100 pA, $20 \times 20\,\mathrm{nm}^2$).

## 2 Analysis of graphene moiré patterns

### Moiré patterns of monolayer graphene on Pt(111)

The moiré pattern is generated by the superposition of Pt(111) and the monolayer graphene (MLG) lattices. In direct space, $a_{\mathrm{Pt}}$, $a_{\mathrm{C}}$, $\delta$ denote the spatial periods of, respectively, the Pt(111) surface, the graphene lattice, the moiré superstructure. In reciprocal space, the corresponding

lattice vectors are $\mathbf{k}_{\mathrm{Pt}}$, $\mathbf{k}_{\mathrm{C}}$, $\mathbf{k}_{\mathrm{m}}$ with magnitudes $k_{\mathrm{Pt}} = |\mathbf{k}_{\mathrm{Pt}}| = 1/a_{\mathrm{Pt}}$, $k_{\mathrm{C}} = |\mathbf{k}_{\mathrm{C}}| = 1/a_{\mathrm{C}}$, $k_{\mathrm{m}} = |\mathbf{k}_{\mathrm{m}}| = 1/\delta$. The moiré superstructure represents a spatial beating pattern, which may be expressed by [1]

$$\mathbf{k}_{\mathrm{m}} = \mathbf{k}_{\mathrm{C}} - \mathbf{k}_{\mathrm{Pt}}. \tag{S1}$$

with $\vartheta = \angle(\mathbf{k}_{\mathrm{Pt}}, \mathbf{k}_{\mathrm{C}})$ and $\varphi = \angle(\mathbf{k}_{\mathrm{Pt}}, \mathbf{k}_{\mathrm{m}})$ defined as the smallest angles enclosed by the respective lattice orientations (Fig. S1). Due to the hexagonal symmetry of the lattices, $\vartheta$ and $\varphi$ are constrained to the interval $[-30°, 30°]$. Spatial periods and orientations of the moiré pattern may readily be derived from the triangle formed by the three reciprocal lattice vectors (Fig. S1a). Using the law of cosines yields $\delta$ as a function of $\vartheta$,

$$\delta = \sqrt{\frac{1}{a_{\mathrm{C}}^2} + \frac{1}{a_{\mathrm{Pt}}^2} - \frac{2\cos\vartheta}{a_{\mathrm{C}} \cdot a_{\mathrm{Pt}}}}^{-1}. \tag{S2}$$

Possible strain in the graphene sheet can be included by scaling the graphene lattice constant appropriately. Figure 2e of the manuscript shows the resulting $\delta$-versus-$\vartheta$ curves. Since $\delta$ is an even function of $\vartheta$, the interval $\vartheta = [0°, 30°]$ contains all possible moiré patterns.

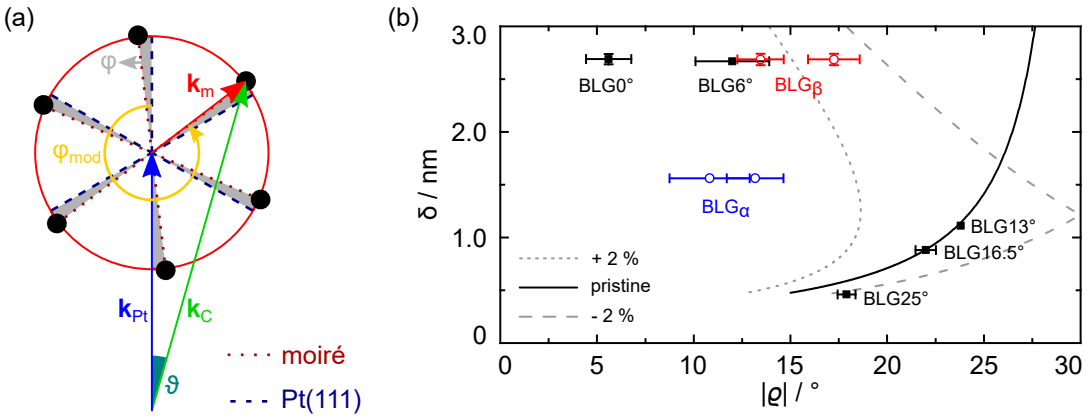


Figure S2: (a) Illustration of the moiré construction. The reciprocal lattice vectors of Pt(111) ($\mathbf{k}_{\mathrm{Pt}}$), graphene ($\mathbf{k}_{\mathrm{C}}$) and the moiré pattern ($\mathbf{k}_{\mathrm{m}}$) form a triangle. The angle enclosed by crystallographic directions of Pt(111) and graphene is denoted as $\vartheta = \angle(\mathbf{k}_{\mathrm{Pt}}, \mathbf{k}_{\mathrm{C}})$, while $\varphi = \angle(\mathbf{k}_{\mathrm{Pt}}, \mathbf{k}_{\mathrm{m}})$ is the angle between crystallographic directions of Pt(111) and the moiré lattice. Dashed and dotted lines represent symmetry directions of, respectively, Pt(111) and the moiré superstructure. Dots on the circle with radius $k_{\mathrm{m}} = |\mathbf{k}_{\mathrm{m}}|$ indicate equivalent moiré superstructures with $\varphi_{\mathrm{mod}} = \varphi + n \cdot 60°$ $(n = 1, 2, \ldots, 5)$, which reproduce the same observable moiré characteristics for varying $\mathbf{k}_{\mathrm{C}}$. (b) Twisted bilayer graphene (BLG) model. Lines depict the calculated moiré spatial period $\delta$ as a function of the angle $\varrho$ enclosed by crystallographic directions of the upper graphene lattice and the moiré superstructure. The solid line shows the variation of $\delta$ with $|\varrho|$ for an unstrained lower graphene sheet, whereas dotted and dashed lines represent the situation for a graphene lattice constant that is increased and decreased by 2 %, respectively. Experimental data appear as circles (this work) and squares (BLG/Ir(111)) [2]. The angles $0° \ldots 25°$ denote the twist angles between the bottom and upper graphene sheets.

## Characterization of the bottom graphene layer in bilayer graphene domains

An important conclusion of the findings presented in the main manuscript is the origin of the moiré pattern observed from bilayer graphene (BLG) domains. The results evidence that the moiré superstructure is caused by the interface beween the bottom graphene layer and Pt(111). Using the moiré characteristics observed from BLG ($BLG_\alpha$, $BLG_\beta$ in Fig. 2e), the spatial period and orientation of the bottom graphene layer may be deduced as follows. Given the spatial moiré period $\delta$ and its orientation $\varphi$ with respect to the Pt(111) lattice, six moiré orientations defined by $\varphi_{\mathrm{mod}}$ in Fig. S1a are indistinguishable in the experiments. These orientations differ by 60°. Free parameters are the unknown orientation of the bottom graphene layer, $\vartheta_{\mathrm{b}}$, and its lattice constant, $a_{\mathrm{C}}$, which may be affected by strain. The solutions with minimal strain are considered most plausible and can be obtained by calculating $a_{\mathrm{C}}$ for every $\varphi_{\mathrm{mod}}$,

$$a_{\mathrm{C}} = \sqrt{\frac{1}{a_{\mathrm{Pt}}^2} + \frac{1}{\delta^2} + \frac{2\cos\varphi_{\mathrm{mod}}}{a_{\mathrm{Pt}}\cdot\delta}}^{-1}. \tag{S3}$$

Subsequently, $\vartheta_{\mathrm{b}}$ is calculated for the selected $a_{\mathrm{C}}^{\mathrm{min}}$ with minimal strain at the angle $\varphi_{\mathrm{mod}}^{\mathrm{min}}$ using

$$\delta \sin\vartheta_{\mathrm{b}} = a_{\mathrm{C}}^{\mathrm{min}} \sin\varphi_{\mathrm{mod}}^{\mathrm{min}}. \tag{S4}$$

Following this procedure, the bottom graphene sheets of the observed BLG domains are characterised by $\vartheta_{\mathrm{b}} = 4.6°$ with $a_{\mathrm{C}} = 240\,\mathrm{pm}$ (−2.5 % strain) in the case of $BLG_\alpha$ and $\vartheta_{\mathrm{b}} = 0.1°$ with $a_{\mathrm{C}} = 252\,\mathrm{pm}$ (2.1 % strain) in the $BLG_\beta$ domain. Consequently, the twist angles $\theta$ between adjacent graphene layers may now be obtained as $\theta = 22.6°$, 13.4° for $BLG_\alpha$ and $\theta = 12.6°$, 18.1° for $BLG_\beta$ subdomains.

## Moiré patterns of twisted bilayer graphene

The moiré pattern generated by twisted BLG can be calculated using Eq. S2 with $a_{\mathrm{Pt}}$ replaced by $a_{\mathrm{C}}$. Thus, the spatial period of a moiré pattern resulting from two unstrained graphene lattices is described by

$$\delta = \frac{a_{\mathrm{C}}}{\sqrt{2(1-\cos\theta)}}. \tag{S5}$$

Assuming that the twist angle between bottom (b) and top (t) graphene sheets causes the observed moiré pattern, b-graphene may be characterised on the basis of this moiré pattern. To this end, t-graphene takes the role of the Pt lattice in Eqs. S3, S4 with known lattice constant $a_{\mathrm{C,t}}$ and as a reference lattice for all angles. The lattice constant $a_{\mathrm{C,b}}$ of the lower graphene is described by

$$a_{\mathrm{C,b}} = \sqrt{\frac{1}{a_{\mathrm{C,t}}^2} + \frac{1}{\delta^2} + \frac{2\cos\varrho_{\mathrm{mod}}}{a_{\mathrm{C,t}}\cdot\delta}} \tag{S6}$$

for each of the six possible orientations defined by $\varrho_{\mathrm{mod}}$, which describes the angle enclosed by the moiré superstructure and t-graphene. The twist angle $\theta$ between the two graphene sheets is then given by

$$\delta \sin\theta = a_{\mathrm{C,b}}^{\mathrm{min}} \sin\varrho_{\mathrm{mod}}^{\mathrm{min}}. \tag{S7}$$

Figure S1b shows BLG data obtained in this work as well as from a recent study of BLG on Ir(111), where the observed moiré patterns were attributed to twisted graphene bilayers[2]. While data for larger twist angles (> 13°) follow the expected behaviour for pristine BLG

reasonably well, there is a notable deviation at smaller rotation angles. Indeed, the BLG0° moiré superstructure is virtually that of the underlying graphene/substrate interface. Density functional calculations[2] showed that low twist angles give rise to an elevated graphene-metal coupling, which is consistent with the mechanism discussed in the main manuscript. In the twisted-BLG model, the $BLG_\alpha$ subdomains (Fig. 3c,d) would require comparably large strains of 3.5 % and 4.2 %, but the $BLG_\beta$ subdomains would exhibit only 1.6 % and 2.3 % strain. However, the resulting moiré patterns of the subdomains would have to align in order to reproduce the experimental observations. Therefore, the twisted-BLG model is not appropriate to explain the observed moiré structures.

## References


[1] A. T. N'Diaye, J. Coraux, T. N. Plasa, C. Busse and T. Michely, *New J. Phys.*, 2008, **10**, 043033.

[2] S. Simon, E. Voloshina, J. Tesch, F. Förschner, V. Enenkel, C. Herbig, T. Knispel, A. Tries, J. Kröger, Y. Dedkov and M. Fonin, *Small*, 2018, **14**, 1703701.